DRAFT VERSION JANUARY 3, 2019
Typeset using LaTeX **twocolumn** style in AASTeX62

Space Telescope and Optical Reverberation Mapping Project. X. The Hidden Life of "the Obscurer" in NGC 5548 and Understanding the Absorption-Line Holiday

M. DEHGHANIAN,[1] G. J. FERLAND,[1] G. A. KRISS,[2] B. M. PETERSON,[2,3,4] S. MATHUR,[3,4] M. MEHDIPOUR,[5] F. GUZMÁN,[1] M. CHATZIKOS,[1] P. A. M. VAN HOOF,[6] R. J. R. WILLIAMS,[7] N. ARAV,[8] A. J. BARTH,[9] M. C. BENTZ,[10] S. BISOGNI,[3,11,12] W. N. BRANDT,[13,14,15] D. M. CRENSHAW,[10] E. DALLA BONTÀ,[16,17] G. DE ROSA,[2] M. M. FAUSNAUGH,[3,18] J. M. GELBORD,[19,20] M. R. GOAD,[21] A. GUPTA,[3] KEITH HORNE,[22] J. KAASTRA,[23,24] C. KNIGGE,[25] K. T. KORISTA,[26] I. M. M$^{\rm c}$HARDY,[25] R. W. POGGE,[3,4] D. A. STARKEY,[22,27] AND M. VESTERGAARD[28,29]

[1]*Department of Physics and Astronomy, The University of Kentucky, Lexington, KY 40506, USA*
[2]*Space Telescope Science Institute, 3700 San Martin Drive, Baltimore, MD 21218, USA*
[3]*Department of Astronomy, The Ohio State University, 140 W 18th Ave, Columbus, OH 43210, USA*
[4]*Center for Cosmology and AstroParticle Physics, The Ohio State University, 191 West Woodruff Ave, Columbus, OH 43210, USA*
[5]*SRON Netherlands Institute for Space Research, Sorbonnelaan 2, 3584, CA Utrecht, The Netherlands*
[6]*Royal Observatory of Belgium, Ringlaan 3, B-1180 Brussels, Belgium*
[7]*AWE plc, Aldermaston, Reading RG7 4PR, UK*
[8]*Department of Physics, Virginia Tech, Blacksburg, VA 24061, USA*
[9]*Department of Physics and Astronomy, 4129 Frederick Reines Hall, University of California, Irvine, CA 92697, USA*
[10]*Department of Physics and Astronomy, Georgia State University, 25 Park Place, Suite 605, Atlanta, GA 30303, USA*
[11]*Osservatorio Astrofisico di Arcetri, largo E. Fermi 5, 50125, Firenze, Italy*
[12]*Harvard-Smithsonian Center for Astrophysics, 60 Garden Street, Cambridge, MA 02138, USA*
[13]*Department of Astronomy and Astrophysics, Eberly College of Science, The Pennsylvania State University, 525 Davey Laboratory, University Park, PA 16802, USA*
[14]*Department of Physics, The Pennsylvania State University, 104 Davey Laboratory, University Park, PA 16802, USA*
[15]*Institute for Gravitation and the Cosmos, The Pennsylvania State University, University Park, PA 16802, USA*
[16]*Dipartimento di Fisica e Astronomia "G. Galilei," Università di Padova, Vicolo dell'Osservatorio 3, I-35122 Padova, Italy*
[17]*INAF-Osservatorio Astronomico di Padova, Vicolo dell'Osservatorio 5 I-35122, Padova, Italy*
[18]*Kavli Institute for Space and Astrophysics Research, Massachusetts Institute of Technology, 77 Massachusetts Avenue, Cambridge, MA 02139-4307, USA*
[19]*Spectral Sciences Inc., 4 Fourth Ave., Burlington, MA 01803, USA*
[20]*Eureka Scientific Inc., 2452 Delmer St. Suite 100, Oakland, CA 94602, USA*
[21]*Department of Physics and Astronomy, University of Leicester, University Road, Leicester, LE1 7RH, UK*
[22]*SUPA Physics and Astronomy, University of St. Andrews, Fife, KY16 9SS Scotland, UK*
[23]*SRON Netherlands Institute for Space Research, Sorbonnelaan 2, 3584 CA Utrecht, The Netherlands*
[24]*Leiden Observatory, Leiden University, PO Box 9513, 2300 RA Leiden, The Netherlands*
[25]*School of Physics and Astronomy, University of Southampton, Highfield, Southampton, SO17 1BJ, UK*
[26]*Department of Physics, Western Michigan University, 1120 Everett Tower, Kalamazoo, MI 49008-5252, USA*
[27]*Department of Astronomy, University of Illinois Urbana-Champaign, 1002 W. Green Street, Urbana, IL 61801, USA*
[28]*Dark Cosmology Centre, Niels Bohr Institute, University of Copenhagen, Vibenshuset, Lyngbyvej 2, DK-2100 Copenhagen Ø, Denmark*
[29]*Steward Observatory, University of Arizona, 933 North Cherry Avenue, Tucson, AZ 85721, USA*

ABSTRACT

The flux variations in the emission lines in active galactic nuclei (AGNs) are driven by variations in the ionizing continuum flux –which are usually reflected in the observable UV-optical continuum. The "Reverberation mapping" technique measures the delay between line and continuum variations to determine the size of the line emitting region; this is the basis for measurements of the central black hole mass in AGNs. The Space Telescope and Optical Reverberation Mapping Project (AGN STORM) on NGC 5548 in 2014 is the most intensive multi-wavelength AGN monitoring campaign ever. For most of the campaign, the emission-line variations followed changes in the continuum with a time lag, as expected. However, the lines varied independently of the observed UV-optical continuum during a 60 – 70 day "holiday." To understand this remarkable phenomenon, we study the intrinsic absorption lines present in NGC 5548. We identify a novel cycle that reproduces the absorption line variability and thus identify the physics that allows the holiday to occur. In our model, variations in this obscurer's line-of-sight covering factor modify the soft X-ray continuum. This leads to changes in the ionization of helium gas in the broad-line region. Ionizing radiation produced by recombining helium then affects the ionization of other species as observed during the AGN STORM holiday. It is likely that any other model which

selectively changes the soft X-ray part of the continuum during the holiday can also explain the anomalous emission line behavior observed.

Keywords: galaxies: active – galaxies: individual (NGC 5548) – galaxies: nuclei – galaxies: Seyfert – line: formation

1. INTRODUCTION

It is now believed that supermassive black holes ($M > 10^6 M_\odot$) reside in the cores of all, or nearly all, massive galaxies. Active galactic nuclei (AGNs) are those supermassive black holes that are accreting mass at high rates relative to the Eddington limit. Rapid gas flows in AGNs are observed as prominent broad emission lines in the ultraviolet (UV) to infrared spectra of these sources, and as strong absorption features seen in the X-rays and the UV. Both the emission and absorption lines are known to vary in strength with time. A long-standing goal of AGN research has been to understand the gas flows in AGN; clearly, accreted gas powers the AGN itself and outflows must interact with the surrounding galaxy, and the details of these interactions have implications for galaxy evolution.

Unfortunately, the gas flows within the black hole radius of influence are generally unresolved, which complicates our attempt to understand their structure and interactions; the broad-line region (BLR), in particular, extends an angle of only ~ 0.1 mas even for the nearest AGNs. We can, however, use temporal variations as a tool to study these otherwise unresolvable flows and structures. The continuum emission that originates in the accretion disk surrounding the black hole undergoes irregular flux variations. The broad emission-line fluxes change in response to these variations, but with a time delay due to the light-travel time between the accretion disk and the BLR; measurement of these time delays is the fundamental goal that underlies the technique of reverberation mapping (Blandford & McKee 1982; Peterson 1993). Similarly, changes in absorption features allow us to make inferences about changes in the AGN spectral energy distribution as well as the ionization state, temperature, and density of the absorbing gas, and other characteristics. In this paper, we will attempt to combine information from reverberation mapping and absorption-line variability to study the structure of the central regions of the nearby ($z = 0.01717$) AGN NGC 5548.

The Seyfert 1 galaxy NGC 5548 was one of the first AGNs in which broad emission-line flux variability was detected (Peterson et al. 1982; Stirpe, de Bruyn, & van Groningen 1988) and one of the first AGNs for which extended monitoring campaigns were undertaken (Peterson 1987; Netzer et al. 1990; Peterson et al. 1990; Rosenblatt & Malkan 1990; Wamsteker et al. 1990) These studies provided the impetus for a major ultraviolet spectroscopic reverberation-mapping campaign by the International AGN Watch consortium using the *International Ultraviolet Explorer* (Clavel et al. 1991). This was accompanied by a similar ground-based program of optical spectroscopic monitoring (Peterson et al. 1991; Dietrich et al. 1993) that triggered a 13–year continuing program (Peterson et al. 1992, 1994, 1999, 2002), as well as a second ultraviolet campaign using the *Hubble Space Telescope* (Korista et al. 1995) and the *Extreme Ultraviolet Explorer* (Marshall et al. 1997). NGC 5548 was included in subsequent reverberation-mapping campaigns led by the Ohio State AGN group (Bentz et al. 2007; Denney et al. 2010; De Rosa et al. 2018) and by the Lick AGN Monitoring Program (LAMP) (Bentz et al. 2009, 2010). NGC 5548 thus provided a unique long-term baseline for exploring the time-dependence of the reverberation phenomenon, as well as a test of reverberation results that ought to be immutable over time (e.g., the black hole mass). Some particularly important results from these extended campaigns included:

- Different emission lines have different response times. Lines characteristic of highly ionized gas vary with a smaller time delay than lines that arise in gas in lower ionization states, i.e., the BLR shows ionization stratification.

- The time lag associated with a particular emission line increases as the mean continuum flux increases. The best-monitored emission line, Hβ, shows time lags as short as a few days and as long as several weeks, depending on the mean luminosity of the AGN during the observing campaign.

- On account of the large number of independent measurements of multiple broad emission lines, NGC 5548 provided the first clear evidence of a relationship between emission-line width and reverberation lag that then enabled determination of the central black hole mass (Peterson & Wandel 1999).

In 2013, NGC 5548 was the subject of an intensive monitoring campaign based primarily on X-ray data from *XMM–Newton* and the *Neil Gehrels Swift Observatory*, supplemented with spectra from the *Hubble Space Telescope* Cosmic Origins Spectrograph (Kaastra et al. 2014; Mehdipour et al. 2015, 2016; Arav et al. 2015; Ursini et al. 2015; Di Gesu et al. 2015; Whewell et al. 2015; Ebrero et al. 2016; Cappi et al. 2016). In the following year, an intensive ultraviolet and optical reverberation-mapping program (the Space Telescope and Optical Reverberation Mapping program, or AGN STORM) was undertaken using *Hubble Space Telescope* (DeRosa et al. 2015; Kriss et al. 2018), the *Neil Gehrels Swift Observatory* (Edelson et al. 2015), ground-based telescopes for both imaging (Fausnaugh et al. 2016) and spectroscopy (Pei et al. 2017), and the *Chandra X-Ray Observatory* (Mathur et al. 2017). This program yielded the first high-fidelity measurements of interband continuum lags (Edelson et al. 2015; Fausnaugh et al. 2016; Starkey et al. 2017) and some very

surprising emission-line results (Goad et al. 2016; Pei et al. 2017) — in particular, some 60 days into the campaign, the broad emission lines appeared to stop responding strongly to continuum variations. However, by the end of the six-month campaign, the normal relationship between the continuum and broad emission lines appeared to be restored. To the AGN STORM team, it appeared as the BLR had "gone on a holiday' and for that reason, we will continue to refer to the period of anomalous emission-line response as the "BLR holiday."

It was subsequently noted (Kriss et al. 2018) that the behavior of the narrow absorption lines changed during the BLR holiday, with the lower-ionization lines continuing to track the observed UV continuum, but with only decorrelated changes in the higher-ionization absorption lines. These holidays are not a prediction of photoionization theory and the current standard model of the geometry of an AGN. Understanding the physics behind the holiday is essential because line-continuum reverberation is the only direct way to measure the mass of the central black hole, and this method is based on the existence of a correlation between the continuum and broad emission lines. The purpose of this paper is to begin an exploration of the BLR holiday phenomenon by examining the behavior of the narrow absorption lines, drawing extensively from the results obtained during the 2013 *XMM-Newton* program as well as the 2014 AGN STORM campaign. We focus on the absorption lines since the geometry is much simpler than the emission-line geometry. Absorbing gas must lie along our line of sight and the clouds must see the same SED as we do. Later sections discuss the observational constraints on the physics behind the holiday. We identify a novel physical process in which changes in the SED cause changes in the ionization of helium, which then drives the absorption line changes observed by *HST*.

2. THE GEOMETRY AND THE OBSCURER

Historically, our line of sight to the central regions of NGC 5548 has been fairly clear, with no heavy obscuration in soft X-ray. Dramatic changes in the soft X-ray absorption occurred and were interpreted as being due to a cloud, "the obscurer," passing across our line of sight (Kaastra et al. 2014; Mehdipour et al. 2016). Soft X-ray absorption by the obscurer was first observed in 2012 and 2013 (Mehdipour et al. 2016; Arav et al. 2015). Here we briefly summarize the geometry inferred by the *XMM-Newton* "Anatomy" series of papers. Figure 1 shows a sketch of the overall geometry, including the black hole and accretion disk which produce the intrinsic (unobscured) SED. The observer is located in the direction of the *HST* icon.

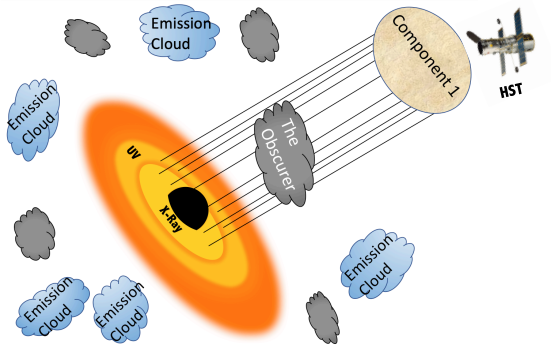

Figure 1. The geometry of the emission and absorption components discussed in this paper. The line of sight obscurer covers 70% to 100% of the X-ray source (Mehdipour et al. 2016). Absorption Component 1 is also shown.

Little is known about the density and location of the obscurer, but the ionization state, inferred high density, the kinematics, absorption line profiles, and the covering factors suggests an origin in the BLR (Kaastra et al. 2014; Di Gesu et al. 2015; Mehdipour et al. 2015). BLR lags of two days to $\sim$ ten days would imply a distance of between $6 \times 10^{15} - 3 \times 10^{16}$ cm (DeRosa et al. 2015). The soft X-ray observations show that the obscurer does not fully cover the X-ray source. The covering factor varied between 0.7 and 1.0 over the period 2012 to 2015 (Mehdipour et al. 2016). This change may be caused by either transverse motions of the obscurer or changes in the size of the X-ray source (Mehdipour et al. 2016). Finally, it is possible that other obscurers lie within the central regions, as shown in Figure 1. Figure 1 also illustrates the cloud producing Component 1 which is the FUV[1] absorption component studied in this paper. Its well-determined distance of 3.5 ± 1.1 pc (Arav et al. 2015) places the Component 1 cloud well outside the BLR but within the narrow-line region (NLR). (Peterson et al. 2013). More details about this component can be found in Arav et al. (2015). In addition, six distinct FUV narrow absorption components were identified by and Crenshaw et al. (2003) and Arav et al. (2015). Component 1 shows the most dramatic changes during the obscuration and was extensively studied by them and by Kriss et al. (2018).

3. THE HOLIDAY

In photoionization equilibrium, there is a one-to-one correlation between the brightness of the ionizing radiation field and the ionization state of the gas. Reverberation measurements rely on this, with the only complication being the time lag caused by the finite speed of light. "Holidays," where the

[1] We refer to the region 6 – 13.6 eV (912 Å to 2000 Å) as FUV; 13.6 – 54.4 eV (228 Å to 912 Å) as EUV; and 54.4 eV to few hundred eV (less than 228 Å) as XUV.

correlation breaks down, are not expected. This section outlines the absorption and emission line holidays that occurred during the AGN STORM campaign.

3.1. *Broad emission lines and their holiday*

The AGN STORM campaign monitored NGC 5548 for the 6-month period from 2014 January to July. During almost 120 days of the campaign, the BLR emission exhibited the expected correlation with the continuum. The line and continuum emission holiday started about 75 days after the first HST observation and continued for 60 to 70 days (Goad et al. 2016). The lines then returned to their normal behavior. Goad et al. (2016) and Pei et al. (2017) note that the strong and broad FUV emission lines became significantly fainter (e.g. in CIV) during the holiday .This is the first observation of such an anomalous behavior in an AGN reverberation mapping campaign.

3.2. *Narrow absorption lines and their holiday*

Some, but not all, of the Component 1 absorption lines displayed a holiday similar to the emission lines. Three low-ionization species — H I, Si II, and C II — showed good correlations with the *HST* FUV continuum, while the higher-ionization species — Si III, Si IV, C III, C IV, and N V — showed decorrelated behavior (Kriss et al. 2018). Figure 2 shows examples of both behaviors, Lyα and N V λ1238. The red line shows the arbitrarily scaled *HST* FUV continuum while the blue lines are Component 1 absorption line equivalent widths (EW). Both lines correlate for most of the campaign, but, like the broad emission lines, there is an almost 70-day period when N V is decorrelated.

3.3. *The scope of this paper*

This paper focuses on the absorption line holiday with the aim of reproducing the correlation / decorrelation shown in Figure 2. As Figure1 shows, the absorption lines involve an especially simple geometry with the continuum emitters and absorbers lying along a single line of sight and the absorbing clouds being illuminated by the SED directed towards the Earth. The absorption lines vary due to changes in the SED striking Component 1. These changes may be due to variations of the brightness of the AGN or changes in the shape of the SED caused by changes in the obscurer's absorption.

The emission lines are more complicated. They might not be directly affected by the obscurer since they lie along different sight lines from the AGN (Figure 1). Other obscurers may be present on other sight lines and could affect the emission lines. The emitting clouds have a range of densities and distances from the center. All of this introduces complexities. The absorption lines are the simplest, and so the best place to start studying the physics behind the holiday. They are the focus of this paper.

The remainder of the paper examines how an absorption line holiday can occur. Our goal is to identify a physical process whereby lines sometime correlate with the observed FUV continuum, and at other times do not. We aim to identify the phenomenology that makes this possible, but not model any particular HST observation. Converting between observed equivalent widths and the ionic column densities we predict requires a curve of growth analysis. This brings in additional uncertainties including the velocity field of the gas and possible substructure within the absorption lines. The presence or absence of a correlation between the FUV continuum and a line equivalent width or column density will not be affected by curve of growth effects. In other words, we want to reproduce the correlation / decorrelation of the lines and continuum and do not model specific derived column densities. We build upon the Arav et al. (2015) model of Component 1 and do not change its basic assumptions.

4. THE "STANDARD" MODEL OF COMPONENT 1

Below we use photoionization models to investigate why some absorption lines correlate with the FUV continuum and some do not. We first adopt the intrinsic SED emitted by the accretion disk, shown in Figure 3. This was derived by continuum modeling during the multi-wavelength campaign data on NGC 5548 (Mehdipour et al. 2015) and is used in all calculations presented below. This SED was incorporated into the developmental version of `cloudy`, most recently described by Ferland et al. (2017), and will be available in the next release. We use this developmental version throughout this paper. Version 17, the latest public release of `cloudy`, included an NGC 5548 SED derived by Tek P. Adhikari from CAMK (Warsaw), by digitizing figure 10 of Mehdipour et al. (2015). That SED did not include data for energies not included in the published figure. The improved SED used by Mehdipour et al. (2015) covers the entire electromagnetic spectrum, and includes the observed Fe Kα line.

We adopt the obscurer parameters — $N(\mathrm{H}) = 1.2 \times 10^{22}\,\mathrm{cm}^{-2}$ and $\log \xi = -1.2$ (erg cm s^{-1}) — derived by Kaastra et al. (2014). The ionization parameter ξ is defined as (Tarter, Tucker, & Salpeter 1969; Kallman & Bautista 2001)

$$\xi = \frac{L}{n(\mathrm{H})R^2}, \tag{1}$$

where L is the luminosity of the ionizing source over the 1–1000 Ryd (13.6 eV to 13.6 keV) band in erg s^{-1}, R is the distance from the source in cm. For the hydrogen density, we adopt $n(\mathrm{H}) = 10^{10}$ cm^{-3} , which is a typical BLR cloud density. We adopt the `cloudy` default value[2] for solar abundances, which are generally within 30% of the Lodders (2003) meteoritic abundances used in some of the previous modeling. The transmitted SED calculated with these parameters is shown in Figure 4, in which we assume that the obscurer fully covers the continuum source. This figure shows the net transmitted radiation field at the shielded face of the obscurer. It includes the attenuated incident radiation field produced by the central object along with line and continuum emission produced by the obscurer. The effects of filtering the continuum has been discussed in other literature

[2] More information about the default values can be find here: https://www.nublado.org/wiki/DownloadLinks

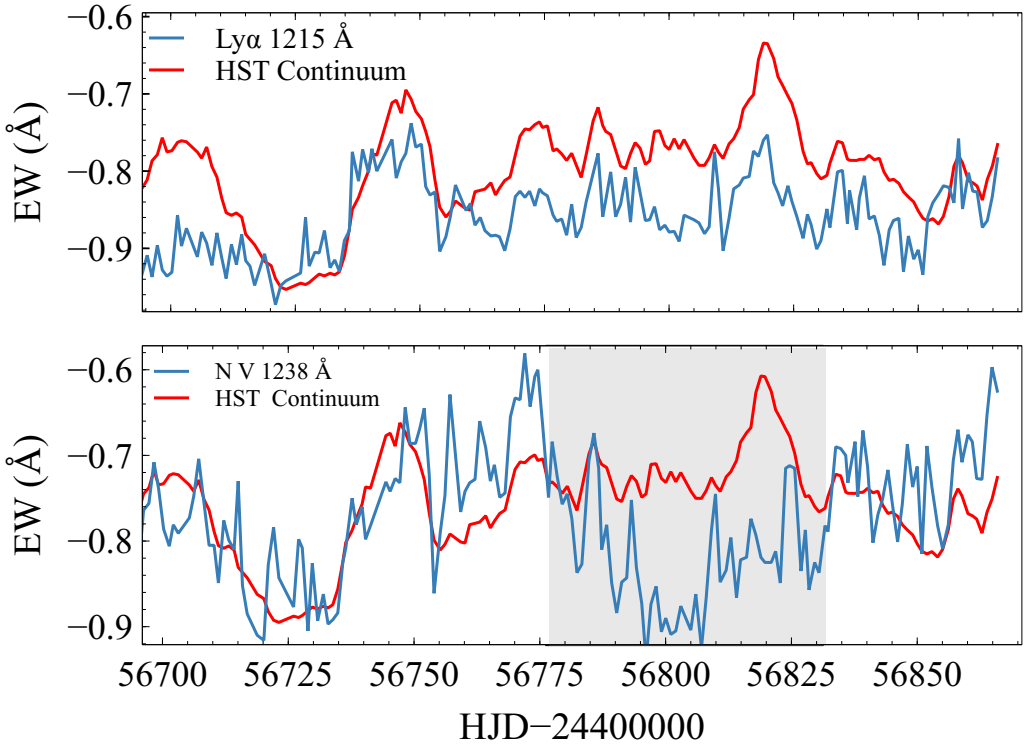

Figure 2. Both panels show the arbitrarily scaled FUV continuum in red, as a function of Heliocentric Julian Date −24400000. The upper panel shows the equivalent width of the Lyα absorber of Component 1 in blue and the lower panel shows the equivalent with of the corresponding N v λ1238. Shaded area indicates the time in which the "holiday" is happening.

but within different contexts (Leighly. 2004). The horizontal lines in Figure 4 indicate the ionization energies for the species studied by Kriss et al. (2018). The left terminus of each line shows the energy needed to produce the ion, while the right terminus indicates the amount of energy required to destroy the ion by further ionization. The high ionization-potential species (indicated by dotted lines) did not correlate with the FUV during the holiday, while lower ionization potential species (solid lines) remained correlated.

In the case of Component 1, we adopt the parameters from Arav et al. (2015), $\log n(\mathrm{H}) = 4.72$ (cm^{-3}) and ionization parameter $\log U = -1.5$, which is defined to be (Osterbrock & Ferland 2006):

$$U = \frac{Q(\mathrm{H})}{4\pi R^2 n(\mathrm{H}) c}, \qquad (2)$$

where $Q(\mathrm{H})$ is the number of hydrogen-ionizing photons emitted by the source per second, R is the cloud distance from the ionizing continuum source, and c is the speed of light. Note that the papers modeling the obscurer (Kaastra et al. 2014) and Component 1 (Arav et al. 2015) use different definitions for the ionization parameter. For the unobscured SED, the relation $\log U = \log \xi - 1.6$ can be used to convert between these ionization parameters. For the obscured SED (Figure 4, green line), the conversion relation is $\log U = \log \xi - 3.3$.

5. WHAT HAPPENED?

We hypothesize that two independent events occurred. First, the luminosity of the AGN varied, causing the entire SED to become brighter or fainter. This would cause the expected correlated variations. Second, the obscurer moved across our line of sight, perhaps due to its orbital motion around the black hole, changing the fraction of the central source that is covered. We will show below that absorption by the obscurer changes the EUV, XUV, and soft X-ray portions of the SED but has little effect on the optical, UV, or FUV, where the obscurer is transparent. This variable absorption, caused by the changing covering factor, would affect the high ionization absorption lines but have little effect on the FUV or optical continuum, so would produce decorrelated changes i.e., a "holiday". In the rest of this section, we investigate these two events in more detail.

5.1. *Changing the luminosity of the source*

The changing luminosity is directly seen via optical, FUV, and X-ray observations. In photoionization equilibrium, this implies a varying ionization parameter, which would change the column densities of all species. As a test, we checked what happens to the column densities of Component 1 absorbing species when the continuum luminosity changes, while keeping the unobscured shape of the SED the same. We use the Arav et al. (2015) standard Component 1 param-

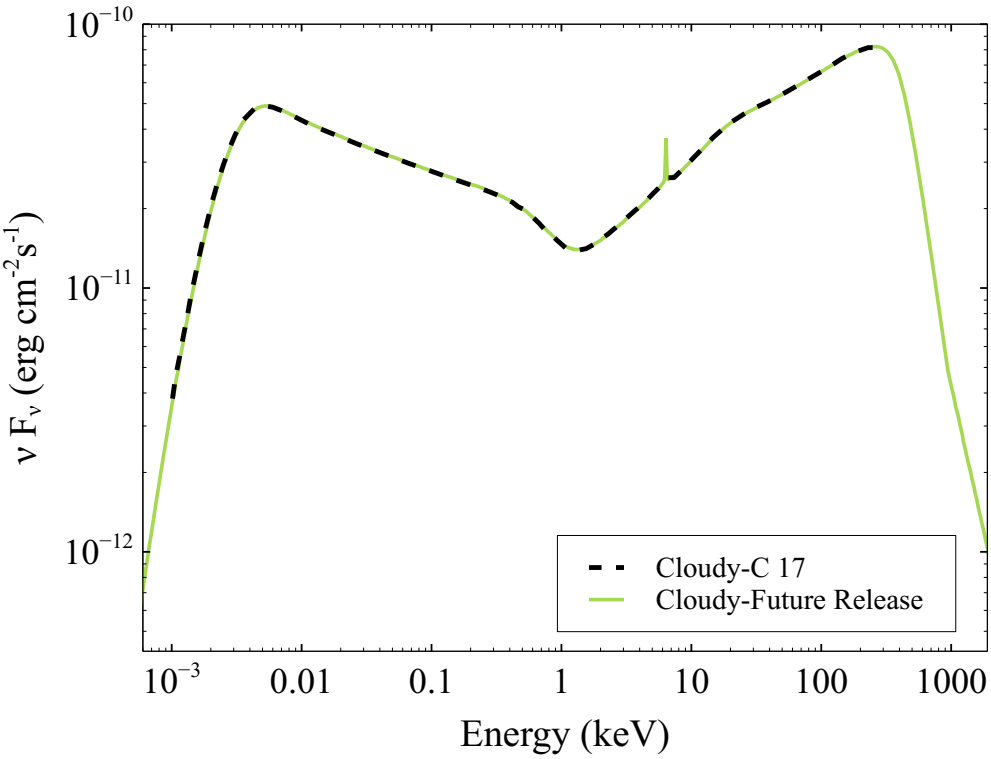

Figure 3. The intrinsic (unobscured) SED available in version 17 of `cloudy` (C17) is shown in dashed-style black line. It was zero outside the indicated range. The green line shows the improved SED (Mehdipour et al. (2015)) which will be implemented in future versions of `cloudy`.

eters as described above, but we let the ionization parameter U vary by one dex to either side of the standard value of $\log U = -1.5$. This would correspond to changes in the continuum luminosity by the same amount. For comparison, the 1157Å *HST* continuum varied over a range of 0.6 dex during the STORM campaign. Figure 5 shows the results of these calculations. The solid lines show the correlated species while the dashed lines are decorrelated. All the column densities change dramatically, however around the standard value of $\log U = -1.5$, the columns of the correlated species are changing very fast, and faster than those of the decorrelated ones. This is not enough to explain the holiday. Thus, simple changes in the luminosity of NGC 5548 cannot explain the absorption line holiday. We must look elsewhere.

5.2. *Changing the obscurer covering factor*

The soft X-ray extinction measures the fraction of the continuum source covered by the obscurer. We refer to this as the "line of sight covering factor" (LOS CF). Changes in the LOS CF affect the absorption lines seen with *HST* since the SED transmitted through the obscurer is responsible for the ionization of Component 1. Figure 6 shows how changes in the LOS CF affects $\mathrm{SED_{inc}}$, the SED striking Component 1. This is defined as:

$$\begin{aligned}\mathrm{SED_{inc}} = &(\mathrm{LOS\ CF}) \times (\mathrm{SED_{extinguished}}) \\ &+(1 - \mathrm{LOS\ CF}) \times \mathrm{SED}\end{aligned} \tag{3}$$

for various LOS CF. Here ?SED? indicates the unattenuated SED shown in Figure 3. The intensity is adjusted to $\log U = -1.5$ with LOS CF = 0 (Arav et al. 2015). We keep the brightness of $\mathrm{SED_{inc}}$ constant at 4558 Å (0.2 Ryd), and vary the LOS CF to obtain different shapes. We chose the energy 0.2 Rydberg since this is an energy where the obscurer is transparent. In Equation (3), LOS CF $= 0$ will be the full unattenuated SED and 100% coverage would be the Mehdipour et al. (2015) extinguished SED (Figure 4). Figure 6 shows that the 1 keV X-ray absorption is highly affected by changes in the LOS CF. The hard X-rays are not absorbed and so do not change. Note that this assumes that the LOS CF is the same for the EUV and XUV, whereas these components may form in different regions (Gardner & Done 2017; Edelson et al. 2018). Note that the SEDs shown in Figure 6 are the *incident* radiation field striking the illuminated face of Component 1. The data come from the second column of the `cloudy save continuum`. The effects of diffuse fields from the obscurer are included when generating the extinguished SED.

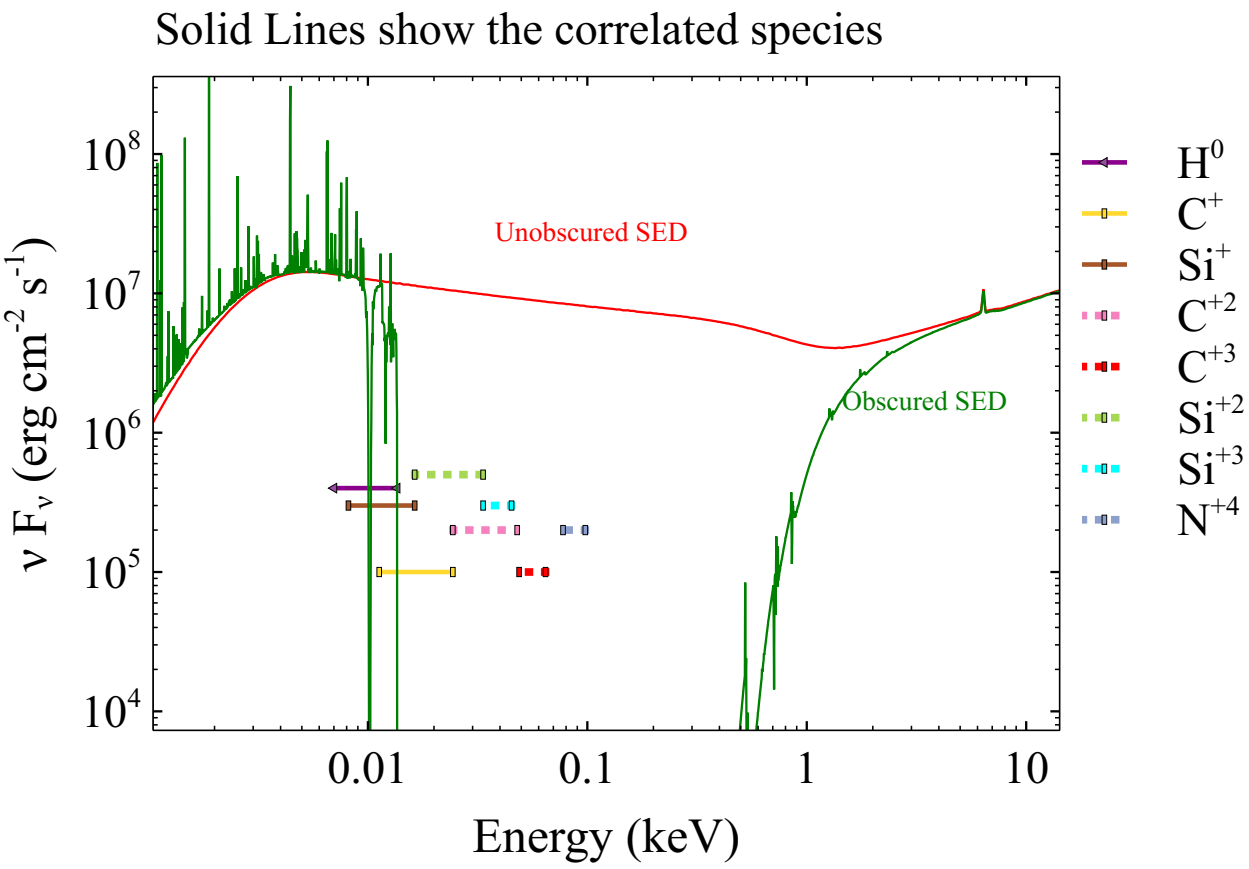

Figure 4. The expected SED transmitted through the obscurer and striking Component 1. Each line segment shows the energy required to produce the ion (left end) and to destroy the ion (right end). In this Figure, we assumed that the obscurer fully covers the continuum source.

Variations of the obscurer LOS CF produce considerable changes in the transmitted SED without producing observable changes in the FUV since the obscurer is transparent in the FUV (see Figure 6). Perhaps this can provide an explanation for the correlated and decorrelated behavior of the narrow absorption lines of Component 1. Next, we investigate how the column densities of Component 1 are affected by the changes in the obscurer LOS CF. We used SEDs like those illustrated in Figure 6 to predict the column densities of the Component 1 species measured by Kriss et al. (2018). These are shown in Figure 7. The column densities of high ionization species decrease while low-ionization species change little at high LOS CF values. Clearly, then, changes in the obscurer LOS CF are capable of causing the absorption line holiday. The next section outlines the physics behind Figure 7.

6. PHYSICS BEHIND THE "HOLIDAY"

Figure 7 focused on the absorption line species observed in the *HST* spectra. These are not necessarily the dominant or most important ions. Figure 8 shows how the physically important ions change, and includes helium, which *HST* did not observe. Silicon and carbon are mainly singly ionized, while He is mostly neutral.

As the LOS CF increases, the column densities of the higher ionization-potential decorrelated ions decrease dramatically, as also seen in Figure 7. The ions He^+ and He^{+2} behave like the higher ionization-potential decorrelated species. Si^+ and C^+ are the most abundant ions, and their column densities do not change. To understand this behavior, we must isolate what photoionizes the dominant and correlated low-ionization species to produce the decorrelated behavior in the higher ionization species. To answer this, we consider the radiation field within Component 1. Figure 9 shows the diffuse radiation field at the midplane, the middle of the Component 1 cloud. The midplane is a representative location, and its properties give insight into the physics of the cloud. We chose a LOS CF of 96%, which is representative of the regions of Figure 7 where the correlated/decorrelated behavior is pronounced. This covering factor is so large that the EUV and XUV portion of the incident SED shown in Figure 6 is faint. The diffuse radiation field shown is produced by emission from the absorbing gas itself and is dominated by line and continuum emission produced by recombining helium. Several of the prominent emission features are la-

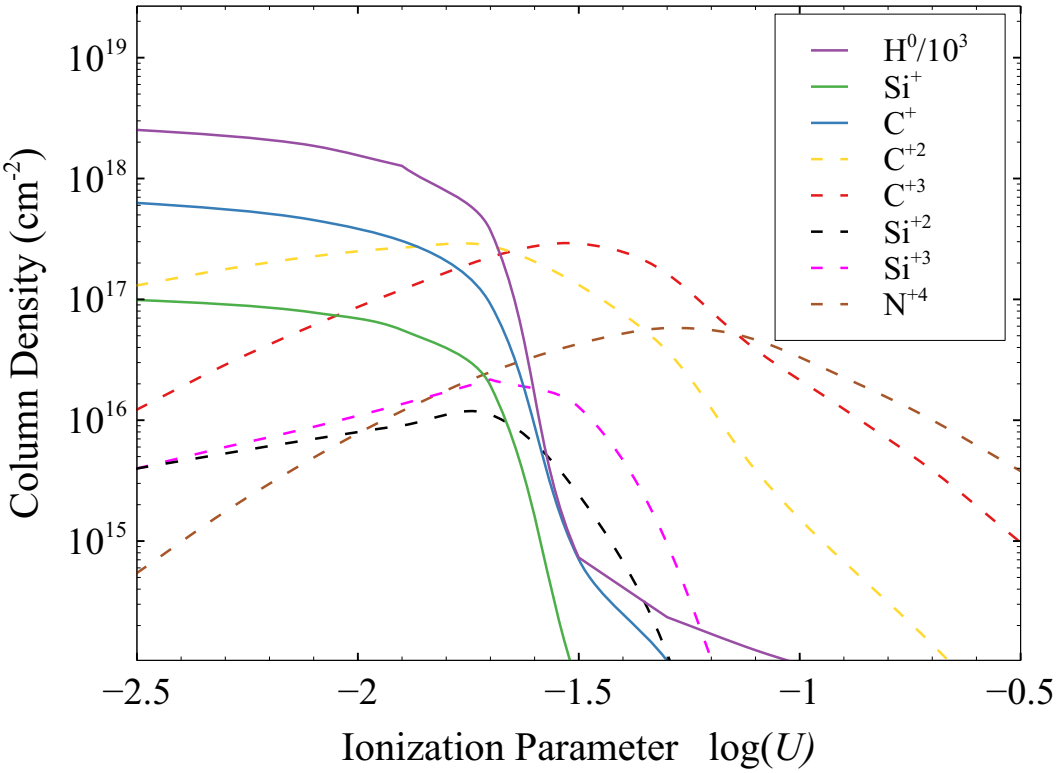

Figure 5. This shows how the Component 1 column densities change as the ionization parameter changes. The hydrogen column density is divided by 1000 to facilitate plotting. The solid lines are correlated species while the dashed lines are decorrelated. These changes are unlike those seen in the holiday, ruling out changes in U as the reason for the holiday.

beled. The horizontal lines indicate the range of photon energy that can photoionize the indicated species.

Examination of the photoionization rates shows that C^+ and Si^+ are produced by photoionization of the neutral atoms by the Balmer continuum. They are destroyed by valence-shell photoionization, with thresholds of 24.4 eV and 16.3 eV for C^+ and Si^+, respectively. Inner shell photoionization by the soft X-rays is much less important. The He I radiative recombination continua (RRC) (for C^+ and Si^+) and singlet and triplet $2p - 1s$ transitions of He^0 (for Si^+) are the primary sources of photoionization at energies of $\sim 20 - 25$ eV, the threshold for destroying these dominant species. These are all produced by recombination of He^+. This means that the abundances of the decorrelated high-ionization species follow the abundance of He^+ and subsequent He I emission. Figure 8 shows that the decrease in column density of the decorrelated species tracks changes in the He^+ column density. What is responsible for photoionization of He^0, producing He^+? He^0 is the dominant ion stage in Component 1 (Figure 8). Examination of the contributors to the photoionization rates shows that He^+ is produced through photoionization by soft X-rays from the attenuated SED of the AGN. Figure 9 shows only the diffuse fields and does not include the attenuated incident SED. He^0 is an important opacity source for soft X-rays. Figure 10 shows the continuous opacity at the midplane of the Component 1 cloud. We evaluated the total gas opacity for the predicted distribution of ions and the assumed solar composition. This shows the opacity per hydrogen and is multiplied by the cube of the photon energy so that it can be compared with standard plots of the total ISM opacity (Ride & Walker 1977). The green line shows the total opacity while the other lines show some of the important contributors to it. H^0 is dominant in the low-energy EUV, He^0 is dominant in the high-energy EUV and XUV, and the heavy elements dominate around 0.5 – 1 keV (Cruddace et al. 1974; Ride & Walker 1977, their figure 2), causing the stepped rise in the right part of the diagram. Helium is mainly neutral (Figure 8) and Figure 10 shows that helium is a major contributor to the total opacity for energies from 24 to 300 eV.

The gas photoionization rate is the integral of the opacity shown in Figure 10 over the radiation field shown in Figure 9 (see Osterbrock & Ferland 2006, equation 2.30). It is critical to know which part of the radiation field dominates the total photoionization rate, since this has the greatest effect on the ionization of Component 1. This is shown in the lower panel of Figure 11. This panel shows the values of the terms entering in the photoionization rate integral, namely the prod-

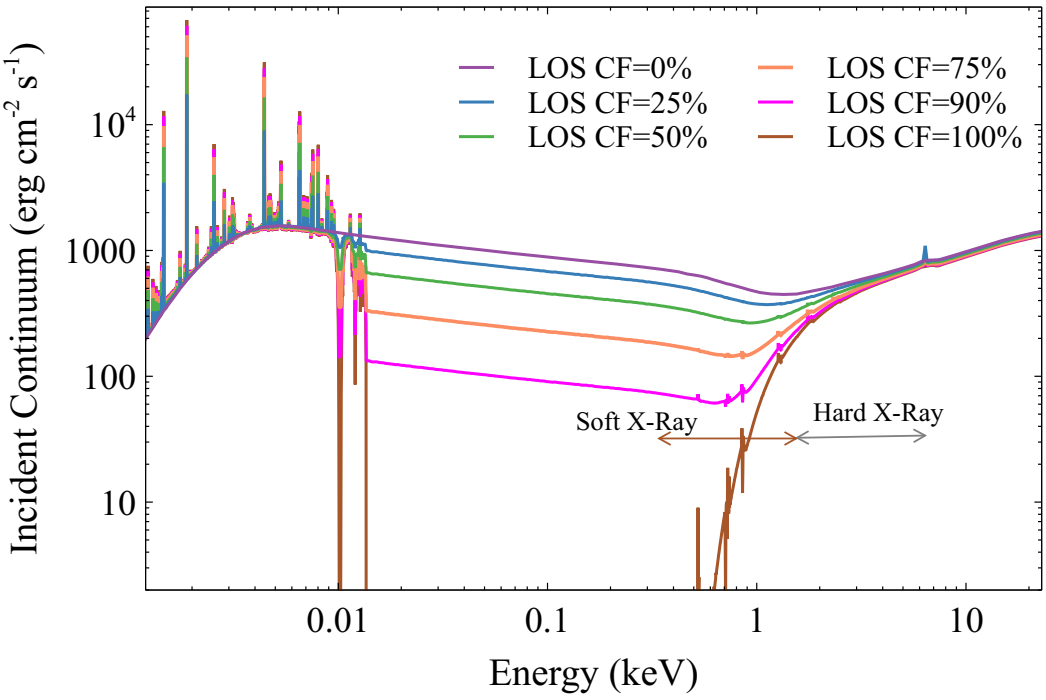

Figure 6. The variations of the SED striking Component 1for different LOS CFs. The Arav et al. (2015) ionization parameter is reproduced at zero coverage. The Figure indicates the soft and hard X-ray energies, i.e., 0.3–0.5 keV and 1.5–10 keV (Mehdipour et al. 2016).

uct $\nu^2\,(4\pi J_\nu/h\nu)\times\alpha_\nu$. In this equation, α_ν is the opacity and J_ν is the mean intensity. This shows the coupling between the radiation and the gas. Only interactions at energies greater than 13.6 eV affect the ionization of the gas, and the strongest coupling occurs at energies between $\sim$ 200 eV to $\sim$ 2 keV. When the LOS CF varies, the soft X-rays change, as shown in Figure 6. This carries over into changes in the ionization of He^0. This leads to changes in the He^0 EUV recombination radiation, which produces the highly ionized species seen by *HST*.

The upper panel of Figure 11 shows the incident SED as a solid blue line. The solid red line shows the total radiation field, including both the diffuse and attenuated incident, at the midplane of Component 1. This is the net transmitted continuum which is the 5th column of the `save continuum` command in `cloudy`. Similar to Figure 6, the effects of diffuse field within the obscurer are included when making a table of the SED passing through the obscurer. We then used this table to generate the appropriate SED in midplane of the Component 1. The EUV and XUV portions of the SED are heavily extinguished so that most radiation at the midplane is due to diffuse gas emission (Figure 9 showed only the diffuse emission).

To summarize, we have investigated, in detail, how changes in the LOS CF affect the ionization of the higher-ionization species observed by *HST* and identified a unique physical cycle. The LOS CF changes the soft X-ray part of the SED but not the FUV continuum, so the resulting changes would not correlate with the FUV. The soft X-rays change the ionization of helium. The ionizing radiation emitted by recombining He^+ changes the ionization rate and abundance of the decorrelated species. However, anything that changes the soft X-rays without affecting the FUV could have a similar effect. This might include the Comptonization scenario outlined by Mathur et al. (2017).

7. TESTING THE COVERING FACTOR MODEL

In this paper, we did not try to model any particular observation but examined how changes in the obscurer can affect parts of the SED and result in the observed correlated/decorrelated behavior. We have identified a physical cycle which can reproduce the observed behavior. Here we outline two observational tests of this model.

7.1. *Existing observations: The X-ray hardness ratio and inferred LOS CF*

Figure 12 summarizes *Swift* and *HST* observations described by Kriss et al. (2018). The red line is the *HST* continuum at 1367 Å, the blue line shows Lyα absorption line and N v absorption line in the upper and lower panels, respectively. These are examples of correlated and decorrelated lines. These are similar to the blue line in the panels of Figure 2. In our model, the changing obscurer covering factor is responsible for the holiday. The X-ray hardness ratio mea-

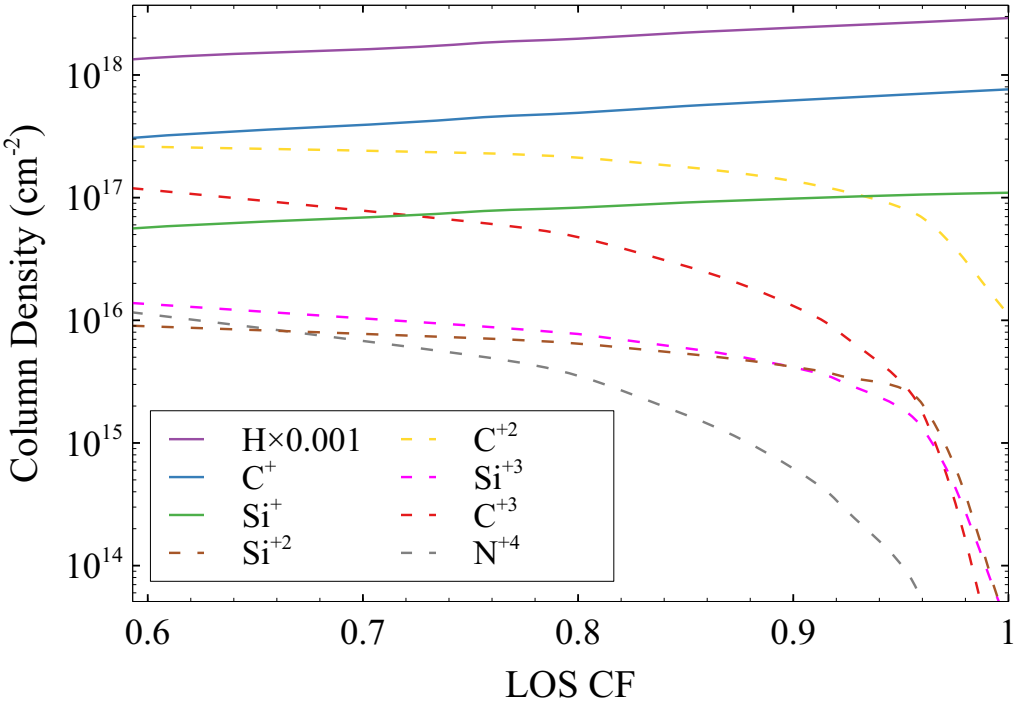

Figure 7. The effects of changes in the obscurer LOS CF upon the column densities observed by *HST*. Low-ionization species (solid lines) remained correlated while high ionization (dashed) species were decorrelated during the holiday, as expected from changes in the obscurer covering factor.

sured by *Swift*, a measure of the hard to soft X-ray brightness, is also a measure of the LOS covering factor, as demonstrated by Mehdipour et al. (2016), equation 2. The obscurer LOS CF changes, derived by Mehdipour et al. (2016) using the broadband spectral modeling of the *Swift* data, are shown in Figure 12 as a green line for comparison. The right CF axis is inverted, decreasing from bottom to top, to make it easier to compare with the other quantities plotted. The upper panel shows that Lyα absorption line is correlated with the *HST* continuum. The LOS CF is also shown in that panel but with a thinner line to not divert attention. The lower panel is drawn similarly, showing that N V absorption line has a better anti-correlation with the LOS CF rather than the correlation with the *HST* continuum.

Figure 12 shows that N V absorption responds to variations of the LOS CF better than the *HST* continuum. Figure 7 shows that larger covering factors and greater extinction cause N V absorption to weaken: N V absorption line is predicted to be anticorrelated with the covering factor. These trends are in the same sense as our predictions.

7.2. *Future observations: the full range of obscurer covering factor*

Figure 7 focuses on large values of the LOS CF because the covering factor was in this range during the holiday (Mehdipour et al. 2016). There were other times when the obscurer was not present. Although this was not observed, there must have been times when the obscurer was first coming into our line of sight, and the LOS CF was increasing from small values. Figure 13 illustrates the full range of the covering factor. The behaviors of the correlated and decorrelated species are reversed for values of LOS CF in the range 0.3-0.5: The correlated species show dramatic changes while the decorrelated ones remain almost constant. Very small values of the LOS CF represented times before 2011 when there was no obscurer. As Figure 13 shows, lower ionization potential species almost disappear. Observations that were performed before 2011 confirm the predictions of Figure 13 (Crenshaw et al. 2009). This motivates future observational tests. Continued monitoring of NGC 5548 by *Swift* could identify times when the LOS CF becomes small again. *HST* observations could then be obtained to follow changes in the absorption lines.

8. SUMMARY

The reverberation mapping method relies on a causal connection between variations in the lines and continuum. This correlation broke down during the so-called 'holiday' period as discovered by the AGN STORM project. The complications due to these abnormalities may have an effect on derived BLR radii and BH masses, this is why it is important

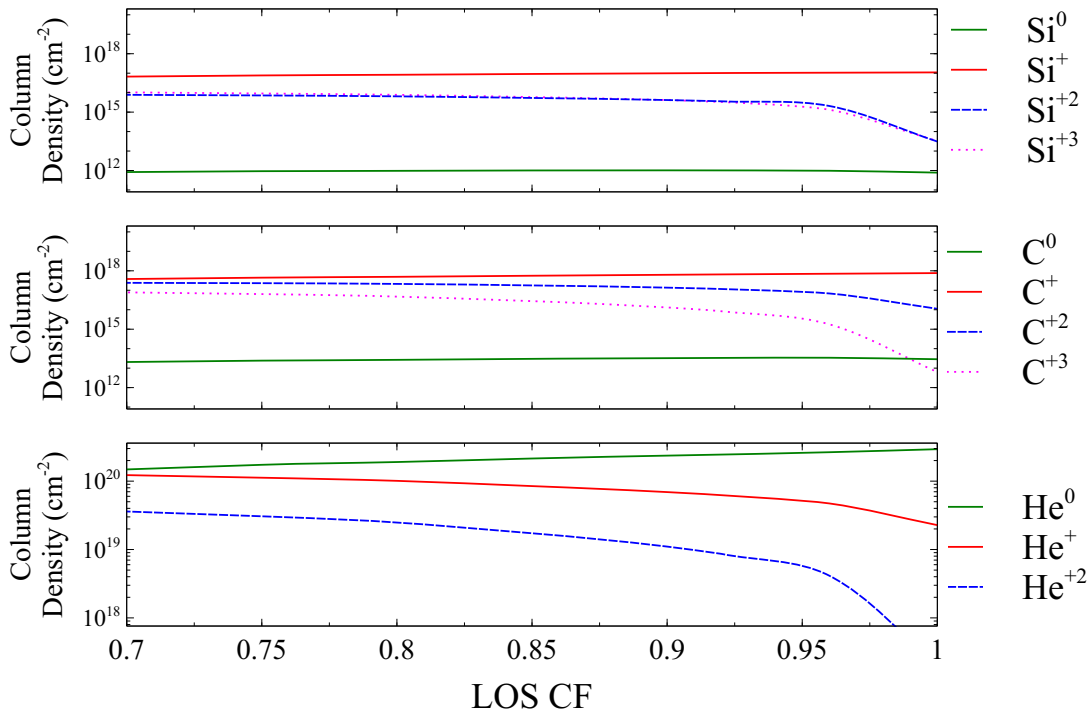

Figure 8. Variations of the column densities of different ionization stages as the obscurer LOS CF changes. Si, C, and He are shown in three panels, from top to bottom, respectively.

to identify the physics which allows such holidays to occur. The fact that high-ionization absorption lines displayed the holiday while low-ionization absorption lines did not is an important clue to what is happening. It is worth emphasizing that "holiday" was first seen in the Broad emission-lines which have a more complicated geometry (Goad et al. 2016). We showed that changes in the luminosity of the AGN do not produce the observed behavior. This suggests that changes in the shape of the SED are responsible. Strong soft X-ray absorption, produced by a transient cloud referred to as the obscurer, was present throughout the AGN STORM campaign. The obscurer covered only a fraction of the continuum source, which we refer to as the "line of sight covering factor," LOS CF. The soft X-ray absorption was not present before 2011, showing that the LOS CF can change dramatically. We investigated the effect of a changing SED on Component 1 cloud producing the strong absorption lines. We have shown that changes in the LOS CF reproduce the observed behavior for large values of the LOS CF. We identified a unique physical cycle in which changes in the LOS CF have a significant effect on soft X-ray portion of the SED. This changes the ionization stage of helium and the ionizing radiation produced as helium recombines drives the changes in the decorrelated absorption lines. Changes in the LOS CF do not affect the optical or UV continuum since the obscurer is transparent that these energies. We identified two tests of this model. The first is the *Swift* measurements of the X-ray hardness ratio. This can be converted into an obscurer covering factor. This LOS covering factor does seem to correlate with the high ionization "decorrelated" absorption lines. We show that the sense of the correlation/decorrelation reverses for smaller covering fractions in the range 0.3-0.5, which can be used to test this scenario in future observations. The tests would have to take place when the covering factor is very low. The photoionization models we produced used a variable covering factor to change the soft X-ray portion of the SED. However, other models in which the soft X-ray part of the SED changes independently of the optical / UV continuum could produce similar effects. The Comptonization model proposed by Mathur et al. (2017) and the Falling Corona Model of Sun et al. (2018) could also produce the required changes in the SED. This will be the subject of future work.

Support for *HST* program number GO-13330 was provided by NASA through a grant from the Space Telescope Science Institute, which is operated by the Association of Universities for Research in Astronomy, Inc., under NASA contract NAS5-26555.We thank NSF (1816537), NASA (ATP 17-0141), and STScI (HST-AR.13914, HST-AR-15018) for their support and Huffaker scholarship for funding the trip to Atlanta to attend the annual AGN STORM meeting, 2017. MC acknowledges support from NASA through STScI grant HST-AR-14556.001-A. M.D. and G.F. and M. acknowledge

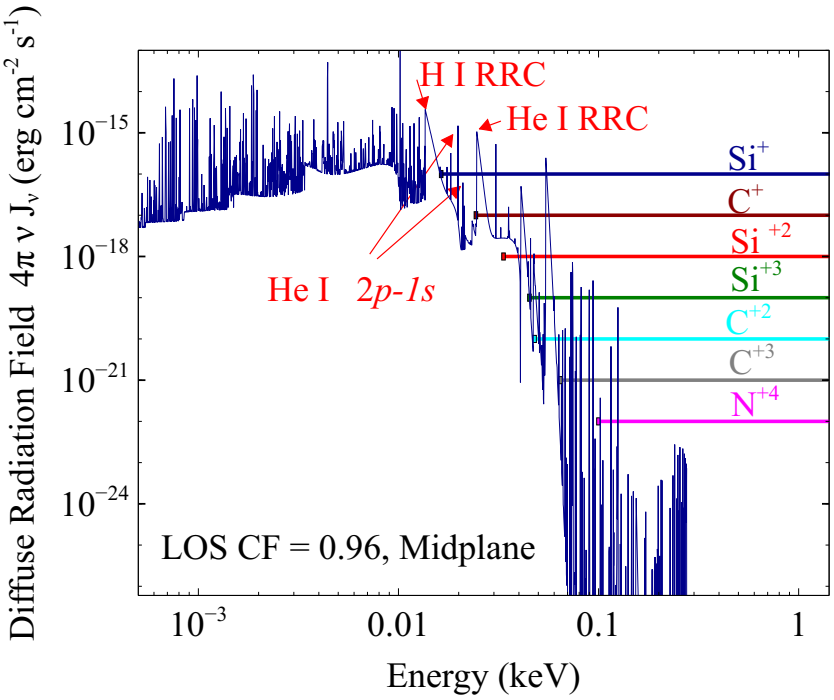

Figure 9. Diffuse emission field at the midplane of Component 1 with 96% obscuration. The left terminus of the horizontal lines shows the minimum energy needed to destroy the ion and produce the higher stage ion. RRC stands for radiative recombination continua.

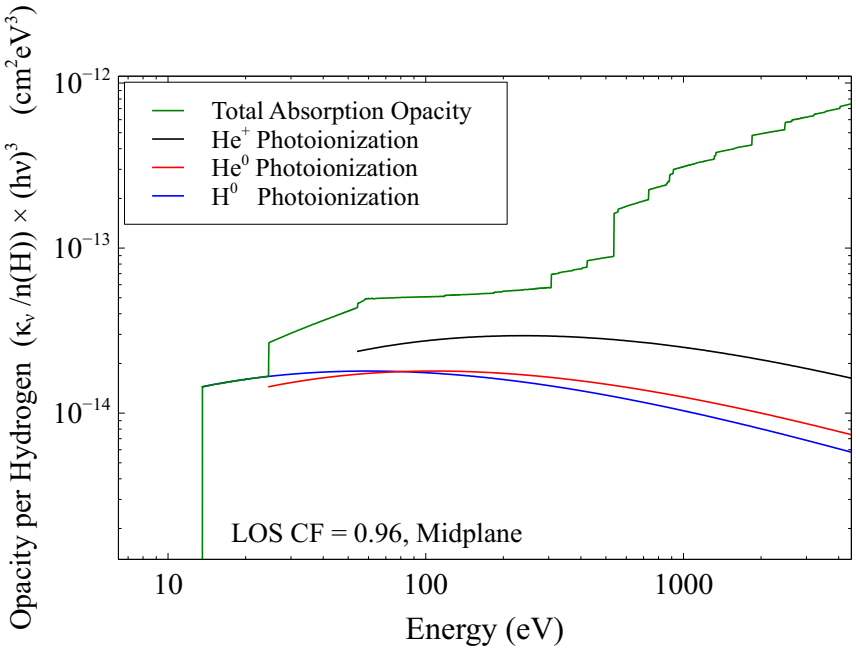

Figure 10. Opacity per hydrogen atom is shown as a function of energy. This shows the total opacity at the Component 1 midplane. The vertical axis has been scaled as described in the text for clarity.

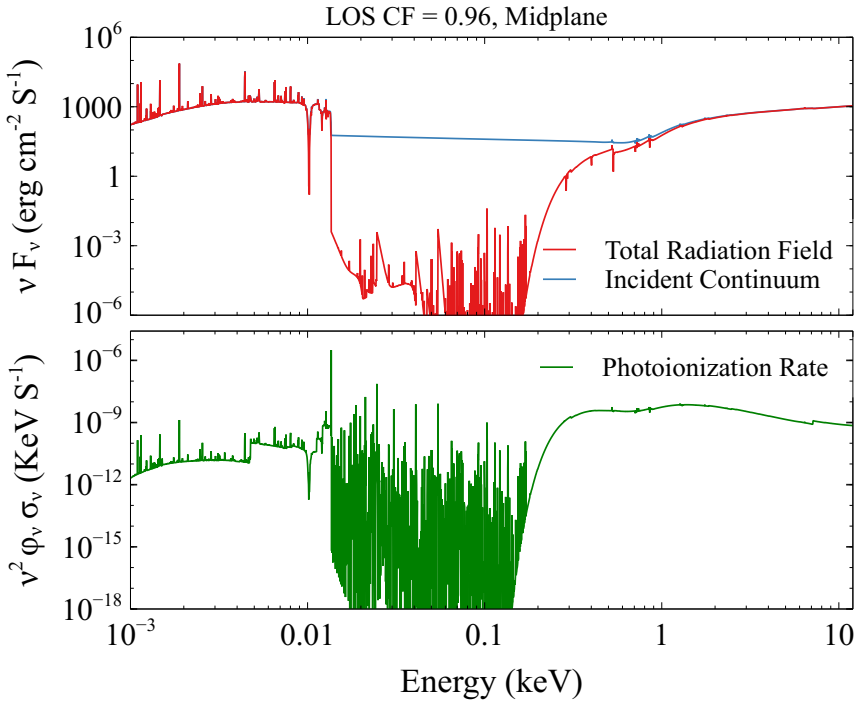

Figure 11. The upper panel shows the radiation field striking Component 1 as the blue line and the radiation field at the midplane of the cloud as the red line. The lower panel shows the photoionization rate at each energy.

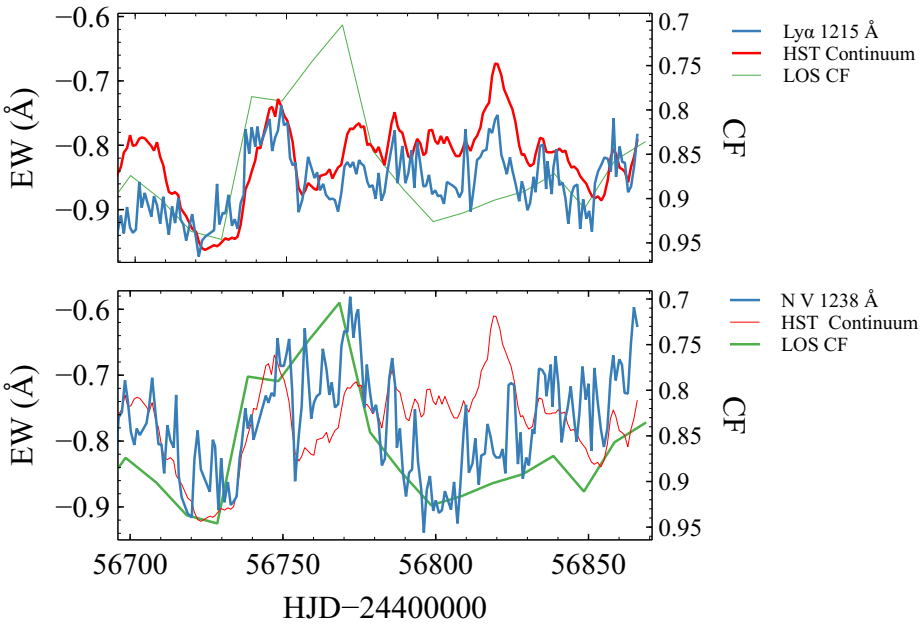

Figure 12. The EW of the Lyα absorption line in Component 1 is shown as the blue line in the upper panel and the EW of the corresponding N V absorption line is shown in the lower panel. The red line shows the *HST* FUV continuum while the green line is the LOS covering factor of the obscurer derived from the X-ray hardness ratio as defined by Mehdipour et al. (2016). Lyα absorption line is correlated with the *HST* continuum while N V absorption line anticorrelates with the covering factor.

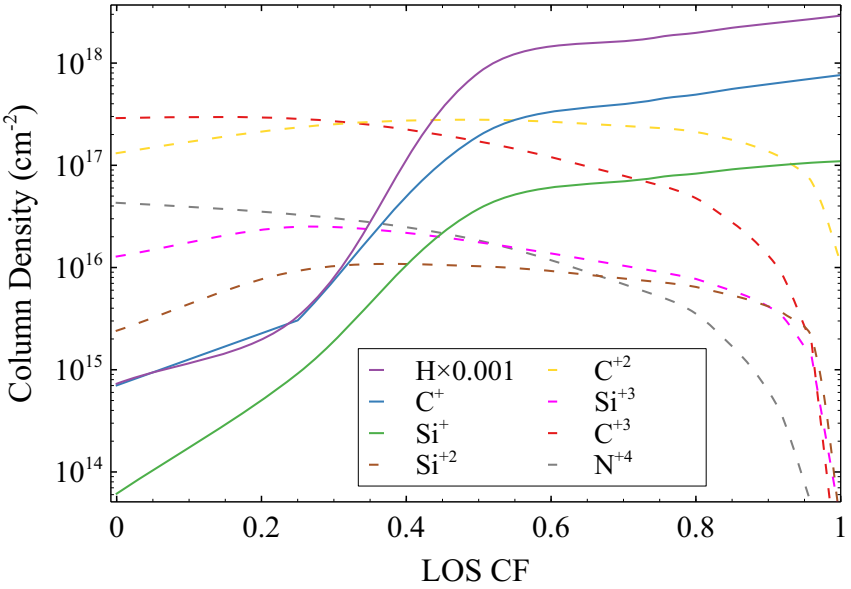

Figure 13. The effects of changes in the LOS CF on the ionic column densities over the full range of covering factor are shown. The dashed and solid lines indicate decorrelated and correlated species, respectively. Their behavior swaps around in the low and high covering factor limits, offering a test of the variable covering factor model.

support from the NSF (AST-1816537), NASA (ATP 17-0141), and STScI (HST-AR-13914, HST-AR-15018), and the Huffaker Scholarship. B.M.P., G.D.R., M.M.F, C.J.G., and R.W.P. are grateful for the support of the National Science Foundation through grant AST-1008882 to The Ohio State University. A.J.B. has been supported by NSF grant AST-1412693. M.C.B. gratefully acknowledges support through NSF CAREER grant AST-1253702 to Georgia State University. S.B. is supported by NASA through the Chandra award no. AR7-18013X issued by the Chandra X-ray Observatory Center, operated by the Smithsonian Astrophysical Observatory for and on behalf of NASA under contract NAS8-03060. S.B. was also partially supported by grant HST-AR-13240.009. E.D.B. acknowledge Ssupport from Padua University through grants DOR1699945/16, DOR1715817/17, DOR1885254/18, and BIRD164402/16. K.D.D. is supported by an NSF Fellowship awarded under grant AST-1302093. R.E. gratefully acknowledges support from NASA under the ADAP award 80NSSC17K0126. K.H. acknowledges support from STFC grant ST/R000824/1. SRON is financially supported by NWO, the Netherlands Organization for Scientific Research. C.S.K. acknowledges the support of NSF grant AST-1009756. A.P. is supported by NASA through Einstein Postdoctoral Fellowship grant number PF5-160141 awarded by the Chandra X-ray Center, which is operated by the Smithsonian Astrophysical Observatory for NASA under contract NAS8-03060. T.T. has been supported by NSF grant AST-1412315. T.T. and B.C.K. acknowledge support from the Packard Foundation in the form of a Packard Research Fellowship to T.T. The American Academy in Rome and the Observatory of Monteporzio Catone are thanked by T.T. for kind hospitality. M.V. gratefully acknowledges support from the Danish Council for Independent Research via grant no. DFF 4002-00275. This research has made use of the NASA/IPAC Extragalactic Database (NED), which is operated by the Jet Propulsion Laboratory, California Institute of Technology, under contract with the National Aeronautics and Space Administration.IMcH acknowledges support from a Royal Society Leverhulme Trust Senior Research Fellowship LT160006 and from STFC grant ST/M001326/1. J.M.G. gratefully acknowledges support from NASA under awards NNX15AH49G and 80NSSC17K0126. E.D.B. acknowledges support from Padua University through grants DOR1699945/16, DOR1715817/17, and DOR1885254/18.

REFERENCES

Arav, N., Chamberlain, C., Kriss, G. A., et al. 2015, A&A 577, 37

Bentz, M.C., Denney, K.D., Cackett, E.M., et al. 2007, ApJ, 662, 205

Bentz, M.C., Walsh, J.L., Barth, A.J., et al. 2009, ApJ, 705, 199

Bentz, M.C., Walsh, J.L., Barth, A.J., et al. 2010, ApJ, 716, 993

Blandford, R.D., & McKee, C.F. 1982, ApJ, 255, 419

Cappi, M., De Marco, B., Ponti, G., et al. 2016, A&A 592, A27

Clavel, J., Reichert, G.A., Alloin, D., et al., 1991, ApJ, 366, 64

Crenshaw, D. M., Kraemer, S. B., et al. 2003, ApJ, 594, 116

Crenshaw, D. M., Kraemer, S. B., et al. 2009, ApJ, 698, 281

Cruddace, R., Paresce, F., Bowyer, S., Lampton, M. 1974, ApJ, 187, 497

Denney, K.D., Peterson, B.M., Pogge, R.W., et al. 2010, ApJ, 721, 715

De Rosa, G., Fausnaugh, M.M., Grier, C.J., et al. 2018, in press (arXiv:1807.04784)

De Rosa, G., Peterson, B. M., Ely, J., et al. 2015, ApJ, 806:128

Dietrich, M., Kollatschny, W., Peterson, B.M., et al., 1993, ApJ, 408, 416

Di Gesu, L., Costantini, E., Ebrero, J., et al. 2015, A&A 579, A42

Ebrero, J., Kaastra, J.S., Kriss, G.A., et al. 2016, A&A, 587, A129

Edelson, R., Gelbord, J. M., Horne, K., et al. 2015, ApJ, 806, 129

Edelson, R., Gelbord, J. M., Cackett, E., et al. 2018, arXiv:1811.07956

Fausnaugh, M. M., Denney, K. D., Barth, A. J., et al. 2016, ApJ, 821, 56

Ferland, G. J., Chatzikos, M., Guzmán, F., et al. 2017, RMxAA, 53,385

Gardner, E. & Done, C. 2017, MNRAS, 470, 3591

Goad, M., Korista, K. T., De Rosa, G., et al. 2016, ApJ, 824, 11

Kaastra, J., S., Kriss, G. A., Cappi, M., et al. 2014, Science, 345, 64

Kallman, T & Bautista, 2001, ApJS, 133, 221

Korista, K.T., Alloin, D., Barr, P., et al. 1995, ApJS, 97, 285

Kriss, G.A., De Rosa, G., Ely, J., et al. 2018, in preparation

Leighly, K.M.2004,ApJ, 611, 125

Lodders, K. 2003, ApJ, 591, 1220

Marshall, H., Carone, T.E., Peterson, B.M., et al. 1997, ApJ, 479, 222

Mathur, S., Gupta, A., Page, K., et al. 2017, ApJ, 846:55

Mehdipour, M., Kaastra, J., S., Kriss, G. A., et al. 2015, A&A, 575, 22

Mehdipour, M., Kaastra, J., S., Kriss, G. A., et al. 2016, A&A, 588, 139

Netzer, H., Maoz, D., Laor, A., et al. 1990, ApJ, 353, 108

Osterbrock D. E., & Ferland G. J., 2006, *Astrophysics of Gaseous Nebulae and Active Galactic Nuclei*, 2nd ed., Univ. Science Books, CA, Herndon, VA

Pei, L., Fausnaugh, M. M., Barth, A. J., et al. 2017, ApJ, 837: 131

Peterson, B.M. 1987, ApJ, 312, 79

Peterson, B.M. 1993, PASP, 105, 247

Peterson, B.M., Alloin, D., Axon, D., et al., 1992, ApJ, 392, 470

Peterson, B.M., Balonek, T.J, Barker, E.S., et al., 1991, ApJ, 368, 119

Peterson, B.M., Barth, A.J., Berlind, R., et al. 1999, ApJ, 510, 659

Peterson, B.M., Berlind, P, Bertram R., et al., 1994, ApJ, 425, 622

Peterson, B.M., Berlind, P., Bertram, R., et al. 2002, ApJ, 581, 197

Peterson, B.M., Denney, K.D., De Rosa, G, Grier, C.J., Pogge, R.W., Bentz, M.C., Kochanek, C.S., Vestergaard, M., Kilerci-Eser, E., Dalla Bontà, E., & Ciroi, S. 2013, ApJ, 779:109

Peterson, B.M., Foltz, C.B., Byard, P.L., & Wagner, R.M. 1982, ApJS, 49, 469

Peterson, B.M., Reichert, G.A., Korista, K.T., & Wagner, R.M. 1990, ApJ, 352, 68

Peterson, B.M., & Wandel, A. 1999, ApJ, 521, L95

Ride, S. K. & Walker, J. R. 1977, A&A, 61, 347

Rosenblatt, E.I., & Malkan, M.A. 1990, ApJ, 350, 132

Starkey, D., Horne, K., Fausnaugh, M. M., et al. 2017, ApJ, 835: 65

Stirpe, G.M., de Bruyn, A.G., & van Groningen, E. 1988, A&A, 200, 9

Sun, M., Xue, Y., Cai, Z.& Guo, H. 2018, ApJ, 857:86

Tarter, C. B., Tucker, W. H. & Salpeter, E. E. 1969, ApJ, 156, 943

Ursini, F., Boissay, R., Petrucci, P.-O., et al. 2015, A&A, 577, A38

Wamsteker, W., Rodriguez-Pascual, P., Wills, B.J., et al. 1990, ApJ, 354, 446

Whewell, M., Branduardi-Raymont, G., Kaastra, J.S., et al. 2015, A&A, 581, A79